

# **Effect of sedimentary heterogeneities in the sealing formation on predictive analysis of geological CO<sub>2</sub> storage**

Michael U. Onoja<sup>a\*</sup>, John D. O. Williams<sup>b</sup>, Hayley Vosper<sup>b</sup>, Seyed M. Shariatipour<sup>a</sup>

<sup>a</sup>Centre for Fluid and Complex Systems, Maudslay House, Coventry University, Coventry, CV1 2NL, United Kingdom.

<sup>b</sup>British Geological Survey, Environmental Science Centre, Keyworth, Nottingham, NG12 5GG, United Kingdom.

\*Corresponding author: [onojau@coventry.ac.uk](mailto:onojau@coventry.ac.uk)

ACCEPTED MANUSCRIPT

## Abstract

Numerical models of geologic carbon sequestration (GCS) in saline aquifers use multiphase fluid flow-characteristic curves (relative permeability and capillary pressure) to represent the interactions of the non-wetting CO<sub>2</sub> and the wetting brine. Relative permeability data for many sedimentary formations is very scarce, resulting in the utilisation of mathematical correlations to generate the fluid flow characteristics in these formations. The flow models are essential for the prediction of CO<sub>2</sub> storage capacity and trapping mechanisms in the geological media. The observation of pressure dissipation across the storage and sealing formations is relevant for storage capacity and geomechanical analysis during CO<sub>2</sub> injection.

This paper evaluates the relevance of representing relative permeability variations in the sealing formation when modelling geological CO<sub>2</sub> sequestration processes. Here we concentrate on gradational changes in the lower part of the caprock, particularly how they affect pressure evolution within the entire sealing formation when duly represented by relative permeability functions.

The results demonstrate the importance of accounting for pore size variations in the mathematical model adopted to generate the characteristic curves for GCS analysis. Gradational changes at the base of the caprock influence the magnitude of pressure that propagates vertically into the caprock from the aquifer, especially at the critical zone (i.e. the region overlying the CO<sub>2</sub> plume accumulating at the reservoir-seal interface). A higher degree of overpressure and CO<sub>2</sub> storage capacity was observed at the base of caprocks that showed gradation. These results illustrate the need to obtain reliable relative permeability functions for GCS, beyond just permeability and porosity data. The study provides a formative principle for geomechanical simulations that study the possibility of pressure-induced caprock failure during CO<sub>2</sub> sequestration.

*Key words:* Geologic carbon sequestration; relative permeability; capillary pressure; pressure evolution; numerical simulation

## 1. Introduction

The geo-sequestration of carbon dioxide (CO<sub>2</sub>) serves as one of the mitigation tools to tackle global warming and has been the subject of extensive research in recent times (IEAGHG, 2017). The main objectives of reservoir engineering studies of CO<sub>2</sub> geo-sequestration include determining reservoir injectivity (André et al., 2014; Miri, 2015), calculating storage capacity (Bachu, 2015; Noy et al., 2012), estimating project costs (Deng et al., 2012; Middleton et al., 2012), evaluating the contribution of different trapping mechanisms (Kaldi et al., 2013; Peters et al., 2015), assessing the risks associated with CO<sub>2</sub> sequestration (Birkholzer et al., 2015; Nicot et al., 2009), and assessing the financial consequences of CO<sub>2</sub> leakage from the geologic repository (Anderson, 2017; Bielicki et al., 2014). These objectives are embodied in the basic metrics for geo-sequestration projects which include the extent of the CO<sub>2</sub> plume migration, formation pressure response, and the measure of immobile and mobile CO<sub>2</sub>.

Consequently, the major requirement for CO<sub>2</sub> geo-sequestration is a suitable underground storage site subjacent to a sufficiently thick and laterally continuous caprock that will prohibit the upward leakage of *in-situ* fluid (Kaldi et al., 2013; Shukla et al., 2011). Among the geological options for CO<sub>2</sub> sequestration, deep saline sedimentary formations offer the highest capacity for storage projects and siliciclastic rocks make up the largest percentage of these formations (IPCC, 2005).

Injecting CO<sub>2</sub> into saline aquifers inevitably results in a multiphase flow of CO<sub>2</sub> and brine. Four recognised geological trapping mechanisms in a CO<sub>2</sub>/brine/rock system are structural/stratigraphic, solubility, residual, and mineralisation (IPCC, 2005). Structural traps function through high capillary entry pressure barriers created by low permeability structures such as caprock formations. Unlike other trapping mechanisms, structural traps do not immobilise CO<sub>2</sub> but rather define the geometry of the formation where more permanent CO<sub>2</sub> storage can occur (Burnside and Naylor, 2014). Structural integrity is an important aspect of geologic carbon sequestration and it relies on the hydromechanical properties of the formation. This is characterised by pressure and strain measurements in both the caprock and the reservoir formation (Khan et al., 2010). Hence, determining the fluid pressure in the caprock is crucial in the identification of hydromechanical processes. The main aim of this study is to provide an accurate and formative principle for geomechanical simulations that study the possibility of pressure-induced caprock failure during CO<sub>2</sub> sequestration.

### 1.1 Structural integrity

CO<sub>2</sub> injection into an aquifer increases the pore pressure which produces an expansion of the aquifer, changing the effective stress field (Ducellier et al., 2011). Due to the coupled hydromechanical effect that occurs during injection, pressure propagates from the aquifer into the caprock hence deforming both formations (Handin et al., 1963). Strain acting laterally can increase lateral stresses while vertically acting strain can be compensated in the form of an extension at the top of the caprock close to the well. The overpressure-induced surface heave observed around injection wells at the In Salah CO<sub>2</sub> storage project in Algeria (Rutqvist et al., 2010) is an example of this vertical strain. The analysis of caprock integrity usually relies on predictions from reservoir and geomechanical models, where the former provides pressure data for the latter. The accuracy of predictions from CO<sub>2</sub> storage simulations is highly dependent on the description of the capillary pressure ( $P_c$ ), wetting saturation ( $S_w$ ), and relative permeability ( $k_r$ ) relationship ( $P_c$ - $S_w$ - $k_r$  relationship) in the flow model (Mori et al., 2015). Due to the lack of experimentally descriptive  $P_c$ - $S_w$ - $k_r$  relationships for saline formations, most numerical models employ constitutive models by Brooks and Corey (1964) or van Genuchten (Van Genuchten, 1980) to describe flow characteristics when simulating geologic CO<sub>2</sub> sequestration (e.g. Cameron and Durlofsky, 2012; Class et al., 2009; Oldenburg et al., 2001). A comprehensive review by Oostrom et al. (2016) highlights the coupled van Genuchten-Mualem-Corey (VGMC) model to be much more efficient in describing the dynamic fluid model. Additionally, a reasonable number of numerical simulations on CO<sub>2</sub> injection into saline aquifer sandstones have utilised this function within a variety of approaches e.g. the hydrodynamic behaviour of CO<sub>2</sub>

(Doughty, 2010), the combined effects of capillary pressure and salinity (Alkan et al., 2010), the effects of interlayer communication through seals (Birkholzer et al., 2009), the major trapping mechanism in Mt. Simon sandstone formation (Liu et al., 2011), the effects of well orientation (Okwen et al., 2011), and the effects of gridding (Yamamoto and Doughty, 2011). Rutqvist and Tsang (2002) showed that hydromechanical changes in the caprock are induced in its basal unit especially in the region near the injection well (injection zone). The authors described a sandstone aquifer beneath a shale caprock using a value of 0.457 to represent the  $VG$ 's pore size distribution index,  $m$ , for both the reservoir and seal formations. Their simulation study, as well as those from aforementioned examples, overlooked the likely importance the interpretation of this parameter,  $m$ , will have on fluid dynamics in sedimentary formations. In a recent study, Shariatipour et al. (2016a) showed that a highly permeable layer at the reservoir-seal interface can contribute to pressure diffusion across the reservoir. The authors indicated that such permeability usually results from weathering, particularly at the unconformity surface, and the reservoir-seal interface could be regarded as a continuing unit of the reservoir's top or the caprock's base. Hence it becomes important that reservoir simulations for  $CO_2$  sequestration adequately describe relative permeability functions at the top of the aquifer and/or the base of the caprock. This is because flow characteristics within either region could differ from the bulk properties of the entire corresponding formation. In this contribution, we focus on the impact of sedimentary heterogeneity, duly represented by intrinsic permeability and relative permeability functions, in the lower part of the caprock on pressure evolution within the sealing formation.

## 1.2. Siliciclastic caprocks

Siliciclastic caprocks are usually composed of fine-grained sediments and commonly referred to as mudrocks in petroleum literature (Folk, 1974; Stow and Piper, 1984). Mudrocks are composed of silt- and clay-sized particles and can be classified as siltstone (with  $> 66\%$  silt-sized particles), mudstone (clay and silt particles between 33% and 66%) or claystone (with  $> 66\%$  clay-sized particles). In describing the fluid model for different mudrocks, petrophysical properties such as porosity and permeability may not be adequate. This is because available laboratory and field data indicate that permeability values can vary by three orders of magnitude for a given porosity and the relative permeability of fluids can also vary at a given permeability for mudrocks (Dewhurst et al., 1999; Yang and Aplin, 2010).

The most efficient mechanism for gas transport through mudrocks is the pressure-driven volume flow of the mobile gas phase (Amann-Hildenbrand et al., 2015). In  $CO_2$ /brine/rock systems, the pressure-driven flow of the mobile gas phase entails visco-capillary two-phase flow which describes the displacement of the wetting brine phase in the original porosity of the rock fabric by the non-wetting gas phase, under the influence of capillary and viscous forces (Bear, 1972). Caprocks possess a smaller pore throat matrix as well as a higher percentage of immobile water within the matrix than reservoir rocks. As such, the capillary entry pressure required to initiate gas flow in water-saturated mudrocks can be extremely high due to the presence of fine-grained

clasts in these rocks (Harrington and Horseman, 1999). Once gas flow is initiated in the porous media, its mobility is usually determined by the permeability of the formation and the  $P_c-S_w-k_r$  relationships. This suggests a functional dependency of pressure distribution, within sedimentary formations, on the rock's microstructural features, such as the pore size distribution or the average grain size composition. In this work a parameterisation scheme by Carsel and Parrish (1988) is used to describe the pore size distribution index,  $m$ , hence the  $P_c-S_w-k_r$  relationship for mudrocks (see Appendix A, Table A1). This is a pragmatic approach, supported by experimental investigations in clastic data sets which show a close relationship between mineralogy, pore throat distributions and capillary function within the rock sample (e.g. Smith et al., 2017). The contribution of other effects such as the wettability of the porous medium and the interfacial tension between the fluids in contact is not considered here.

### 1.3 Problem statement

Generally, gas migration through the water-wet caprock will be initiated when the gas pressure in the reservoir exceeds the capillary entry pressure. Any resulting fracture-controlled flow of CO<sub>2</sub> will be influenced by its effective permeability, which is likely to be higher for silt-rich than clay-rich mudrocks (Dewhurst et al., 1998). However, a common practice in various reservoir modelling studies is the adoption of a single  $P_c-S_w-k_r$  curve for an entire mudrock column overlying a storage formation. This may not always be ideal practice especially for lithostratigraphic units such as the Mercia Mudstone Group (MMG) in the East Irish Sea which is mainly composed of claystones and siltstones (Seedhouse and Racey, 1997). In an experimental investigation of the capillary sealing properties of nine high quality sealing mudrock samples, Amann-Hildendrand et al. (2013) observed that only a small proportion, i.e. a narrow horizontal band, of the rock fabric was exposed to the permeating fluid/CO<sub>2</sub> after the capillary entry pressure was exceeded. This was attributed to the dependency of the effective gas permeability on the capillary pressure curve. At the basin scale, the fraction of rock fabric exposed to the permeating CO<sub>2</sub> could be interpreted as the reservoir/seal interface. Since the capillary pressure-controlled properties are associated with the pore size distribution and wettability, the lithology and mineral composition of the mudrock at the reservoir/seal interface becomes important when estimating the capillary sealing efficiency of the caprock overlying potential CO<sub>2</sub> storage sites. The MMG, which overlies potential CO<sub>2</sub> storage formations such as the Sherwood Sandstone Group and its North Sea equivalent, the Bunter Sandstone Formation (Noy et al., 2012; Williams et al., 2018), equally serves as a good example here. At the reservoir/seal interface, transitional lithologies commonly exist between the Sherwood Sandstone and the Mercia Mudstone (Newell and Shariatipour, 2016; Seedhouse and Racey, 1997; Shariatipour et al., 2016b). This lithology is characterised by interbedded claystone, siltstones and medium- to fine- grained sandstones of approximately equal proportions (Hobbs et al., 2002). Onshore UK, the transitional interface is referred to as the Tarporley Siltstone Formation and forms the basal formation of the Mercia Mudstone Group with gradational changes at its top and base in the East Midlands Shelf (up to 60 m), the Cheshire Basin (up to 220 m), and the Stafford Basin (up to 70 m) (Howard et

al., 2008). With Bennion and Bachu (2008) demonstrating that relative permeabilities for in situ fluids within a storage location can follow different curves, the classical two-phase flow concept in mudrocks may need refining and adapting, with respect to the  $P_c-S_w-k_r$  functions in varying mudrock lithologies that could occur within a sealing formation. In other words, using a single  $P_c-S_w-k_r$  curve in reservoir models to represent the flow characteristics of formations showing lithological gradation will yield significant errors in predictions of fluid flow and pressure response (Zhang et al., 2013).

## 2. Model characteristics

### 2.1 Model description

A two-dimensional (2D) radially symmetric model domain with a radial extent of 6 km was chosen to represent the aquifer-caprock system. This is to investigate the impact of boundary conditions on the results while also ensuring that the mobile CO<sub>2</sub> plume during injection does not reach the lateral boundary of the domain. A storage formation, located at a depth of approximately 1000 m below the ground surface, is 200 m thick and bounded at the top by a 200 m thick caprock sealing unit. The upper and lower boundaries of the domain have no flow conditions. Two observation zones identified as Region 1 and Region 2 (see Fig. 1) are used to represent the zones of reference above the perforated injection interval, as implemented for this study.

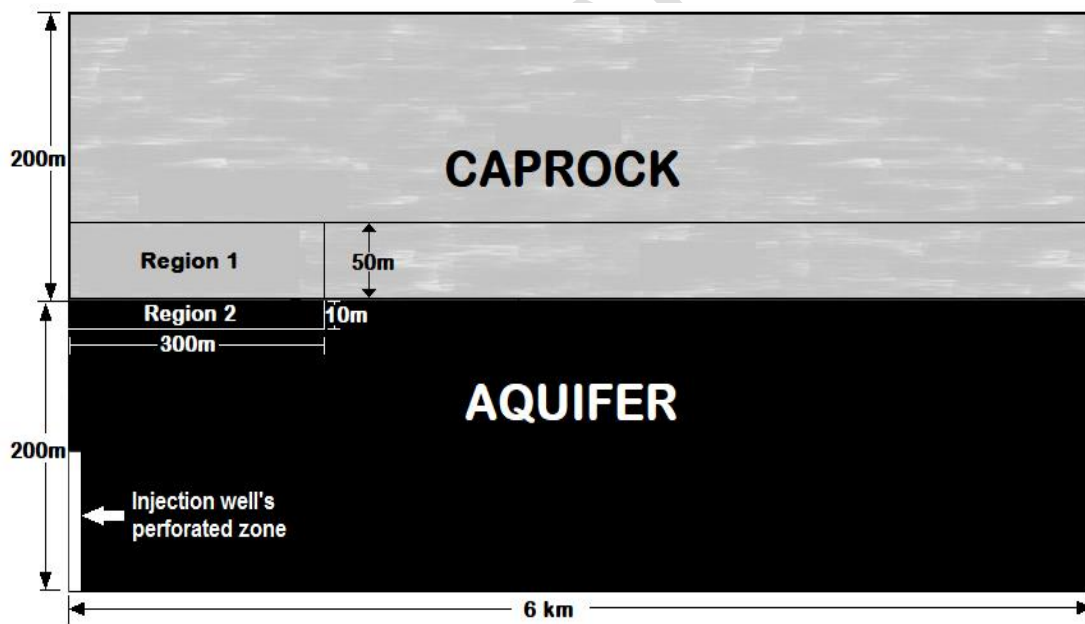


Fig. 1: Schematic description of the model geometry in the r-z cross section, where Regions 1 and 2 are observation zones in the study. *Not to scale.*

A single vertical injection well is located at  $r = 0$  with CO<sub>2</sub> injection operating over 20 years at a rate of 48 kg/s (i.e. annual rate of 1.5 million tonnes of CO<sub>2</sub>). This is equivalent to half of the CO<sub>2</sub> emissions of a 500 MW coal-fired power plant (Orr, 2009). The aquifer is initially fully saturated, assuming a hydrostatic fluid pressure distribution and a salinity of 300,000 ppm. Isothermal conditions are modelled using a uniform temperature of 33°C. Schlumberger's (2015) ECLIPSE multiphase code is used for the dynamic simulation of supercritical CO<sub>2</sub> (scCO<sub>2</sub>) displacing brine. The allowable

bottom-hole-pressure (BHP) is set to 75% of a lithostatic pressure gradient assumed to be 22.5 MPa/km (after Noy et al., 2012). This is ~90% of the minimum horizontal stress magnitude in the East Irish Sea Basin as estimated by Williams et al. (2018). In order to accurately approximate the magnitude of expected fluid pressure increase resulting from CO<sub>2</sub> injection, cells towards the top of the reservoir and at the base of the caprock are thinner. Within the reservoir-seal interval the thinnest cells are 0.01 m thick while the average cell thickness within the model is 1 m. The petrophysical properties of the aquifer are based on the Sherwood Sandstone Group of the South Morecambe gas field in the East Irish Sea Basin (Bastin et al., 2003). Table 1 lists the assigned hydrogeological properties typical of a homogeneous saline aquifer that is suitable for CO<sub>2</sub> storage.

Parameter	Aquifer
Porosity, $\emptyset$ (%)	14
Permeability (mD)	150
Permeability anisotropy	0.1
Gas entry pressure, $P_e$ (kPa)	1.6
Irreducible brine saturation, $S_{wr}$	0.3
Pore compressibility (bar <sup>-1</sup> )	4.5 x 10 <sup>-5</sup>
Maximum relative permeability to CO <sub>2</sub> , $k_o$	0.584

Table 1: Static parameters assumed in the modelled domain

The aquifer is assumed to be a fully water-wet sandstone formation with a maximum pore throat radius of 37 microns and CO<sub>2</sub>/brine interfacial tension of 30 mN/m. The assumed value for maximum pore throat radius falls within the range of dominant pore throat sizes of Permo-Triassic sandstones in the United Kingdom (Bloomfield et al., 2001). The coupled van Genuchten-Mualem-Corey (VGMC) model, where  $m$  and  $n$  are pore geometry parameters related by the assumption that  $m = 1 - 1/n$ , is employed to describe the retention behaviour of the rocks and the relative permeability of brine and CO<sub>2</sub>, using the equations below:

$$P_c = P_g [(S_{ew})^{-1/m} - 1]^{1/n} \quad \text{Eq. 1}$$

$$P_g = \frac{P_e}{(S_{ew})^{1/\lambda} [(S_{ew})^{-1/m} - 1]^{1-m}} \quad \text{Eq. 2}$$

$$\lambda = \frac{m}{1-m} \left(1 - 0.5^{\frac{1}{m}}\right) \quad \text{Eq. 3}$$

$$P_e = \frac{2\sigma \cos\theta}{r_{max}} \quad \text{Eq. 4}$$

$$S_{ew} = \frac{S_w - S_{wr}}{1 - S_{nr} - S_{wr}} \quad \text{Eq. 5}$$

$$k_{rw} = S_{ew}^{1/2} \left[1 - (1 - S_{ew}^{1/m})^m\right]^2 \quad \text{Eq. 6}$$

$$k_{rn} = k_o * [(1 - S_{ew})^2 * (1 - S_{ew}^2)] \quad \text{Eq. 7}$$

where  $P_c$  is the capillary pressure,  $P_g$  is a pressure scaling parameter, which defines the capillary entry pressure,  $P_e$ , required for a non-wetting fluid to displace a wetting fluid in the maximum pore throat radius,  $r_{max}$ , using Eq. 2 and 3 (Lenhard et al., 1989)  $\lambda$  is the pore size distribution index used to fit  $P_e$  into Eq. 1,  $\sigma$  is the interfacial tension

between the wetting and non-wetting fluids,  $\theta$  is the wettability, expressed by the angle of contact which the fluid interface forms with the solid,  $S_{ew}$  is the effective wetting phase saturation,  $S_w$  is the wetting saturation,  $S_{wr}$  is the residual saturation of the wetting phase,  $S_{nr}$  is the residual saturation of the non-wetting phase, which equals zero for the drainage cycle and  $S_{nr,max}$  (i.e. maximum non-wetting saturation) for the imbibition cycle,  $k_{rw}$  is the relative permeability to brine,  $k_m$  is the relative permeability to CO<sub>2</sub>, and  $k_o$  is the maximum relative permeability value for the non-wetting phase.

## 2.2 Sensitivity study design

Using a set of simulation scenarios, the paper aims to evaluate the degree to which a gradation at the base of a sealing caprock will affect the magnitude of pressure that propagates into the sealing formation as a result of scCO<sub>2</sub> injection in the underlying reservoir. For the purpose of this study, the transition zone henceforth refers to the region of gradational changes at the lower part of the caprock. A set of graded orientation identified as coarse- to fine-, fine- to coarse-, and coarse- to fine- to coarse-textured sediments is constructed within a transition zone with varying thickness of 0.1m, 1m, 10m, 20m and 50m. A total of six different caprock lithologies, namely claystone, sandy claystone, mudstone, siltstone, sandy siltstone and clayey sandstone, are used to describe various flow characteristics within the caprock formation. This study identifies claystone, sandy claystone and mudstone as finer lithologies while siltstone, sandy siltstone and clayey sandstone are identified as coarser lithologies. All lithologies are modelled under the assumption of a single value for capillary entry pressure for all variations, i.e. 172 kPa. This is based on the subjective approach that each lithological variation possesses the same diameter of largest pore throat on the exterior of the stratum in contact with the displacing fluid. The pore geometry parameter,  $m$ , then defines the variable capillary breakthrough pressure for each lithological unit (Appendix A, Table A1). Residual CO<sub>2</sub> saturation, an important parameter for imbibition curves to model residual trapping, is not computed for the variable lithologies since the study is focused on the drainage cycle. Assumed values for residual brine saturation are based on Bennion and Bachu's (2008) experimentally measured relative permeability characteristics for supercritical CO<sub>2</sub> displacing brine from low permeable shale, carbonate and limestone rock samples. Endpoint CO<sub>2</sub> relative permeabilities, i.e. the maximum relative permeability to the non-wetting phase, are computed using the following relationship proposed by Standing (1975):

$$k_o = 1.31 - (2.62 * S_{wr}) + (1.1 * S_{wr}^2) \quad \text{Eq. 8}$$

The heterogeneous properties of the caprock lithologies are listed in Table 2 where a single porosity of 4.4% is assumed for the caprock lithologies with permeability values ranging from  $2.23 \times 10^{-4}$  mD to  $7.88 \times 10^{-5}$  mD, linearly characterised by their clay content. This hypothesis is supported by existing data that suggests a log-linear relationship between permeability and porosity over a wide range of mudstones with dataset of measured permeabilities spanning approximately 1 order of magnitude at a single porosity value provided the clay content and mean pore throat radius of the mudstones are known (Yang and Aplin, 2010, 2007). Armitage et al. (2016) further



demonstrated that the lower the clay content, the higher the permeability at the same porosity, and provided a compilation of Kv/Kh ratio for six Mercia Mudstone core samples which vary between 0.493 and 0.852. Based on this range, the permeability anisotropy in the caprock is assumed to be 0.5. Relative permeability ( $k_r$ ) – Saturation ( $S$ ) relations used in the numerical simulations are shown in Appendix A (Fig. A3).

Caprock lithology	<i>van Genuchten pore size distribution parameter, m</i> (where $m = 1 - 1/n$ )	Intrinsic Permeability, K (mD)	Residual brine saturation ( $S_{wr}$ )	Maximum relative permeability to CO <sub>2</sub> ( $k_o$ )
Claystone	0.083	$7.88 \times 10^{-5}$	0.605	0.128
Sandy Claystone	0.187	$4.23 \times 10^{-5}$	0.595	0.141
Mudstone	0.237	$1.72 \times 10^{-5}$	0.569	0.175
Siltstone	0.270	$8.21 \times 10^{-4}$	0.558	0.191
Sandy Siltstone	0.291	$5.37 \times 10^{-4}$	0.492	0.287
Clayey Sandstone	0.324	$2.23 \times 10^{-4}$	0.476	0.312

Table 2: Heterogeneous properties of the caprock lithologies

In accordance with the  $k_r$ – $S$  functions computed for the caprock lithologies, claystone is regarded as the most compact lithology with the highest impedance on fluid flow, followed by sandy claystone then mudstone, siltstone, sandy siltstone and finally clayey sandstone. All properties of the reservoir are identical in all the sensitivity cases while the caprock lithologies within the basal transition zone are modelled with an equal fraction of thickness for each case. Sensitivity simulations conducted in this study are listed in Table 3.

Case ID	CAPROCK		
	<i>Extensive top unit (m)</i>	<i>Basal transition unit (m)</i>	<i>Lithology from the top to base</i>
BASE	200	0	Claystone
CASE1_0.1m	199.9	0.1	Claystone (Top unit) Sandy Claystone Mudstone Siltstone Sandy Siltstone Clayey Sandstone
CASE1_1m	199	1	
CASE1_10m	190	10	
CASE1_20m	180	20	
CASE1_50m	150	50	
CASE2_0.1m	199.9	0.1	
CASE2_1m	199	1	
CASE2_10m	190	10	
CASE2_20m	180	20	
CASE2_50m	150	50	

CASE3_0.1m	199.9	0.1	Claystone (Top unit) Sandy Claystone Mudstone Siltstone Sandy Siltstone Clayey Sandstone Sandy Siltstone Siltstone Mudstone Sandy Claystone Claystone
CASE3_1m	199	1	
CASE3_10m	190	10	
CASE3_20m	180	20	
CASE3_50m	150	50	
CASE4_0.1m	199.9	0.1	Claystone (Top unit) Sandy Siltstone Siltstone Mudstone Sandy Claystone Claystone Sandy Claystone Mudstone Siltstone Sandy Siltstone Clayey Sandstone
CASE4_1m	199	1	
CASE4_10m	190	10	
CASE4_20m	180	20	
CASE4_50m	150	50	

Table 3: Description of the primary sensitivity simulations conducted in the study. *NB: The lithologies at the basal transition interface of cases 1-4 have an equal fraction of thickness.*

### 3. Results and discussion

In order to compare the pressure profile for a caprock with a basal transition zone against one without, numerical simulations of CO<sub>2</sub> injection into an underlying homogenous aquifer are initiated within closed and open boundary conditions. Modelling of the closed and open systems entail no-flow conditions and flow conditions at the 6 km lateral boundary, respectively. Simulations are run within two different scenarios; the first defines sedimentary heterogeneities in the basal transition zone of the caprock using relative and intrinsic permeability values, herein identified as “ $K + k_r$ ”, while the second defines heterogeneity using only intrinsic permeability values, herein identified as “*only K*”. This is done to compare the influence of parametric representation of heterogeneity on the predictive analysis of caprock pressurisation during CO<sub>2</sub> storage. The results are analysed below.

#### 3.1 Closed system

The CO<sub>2</sub> saturations within the reservoir for all the sensitivity cases of the model are practically identical and presented in Fig. 2:

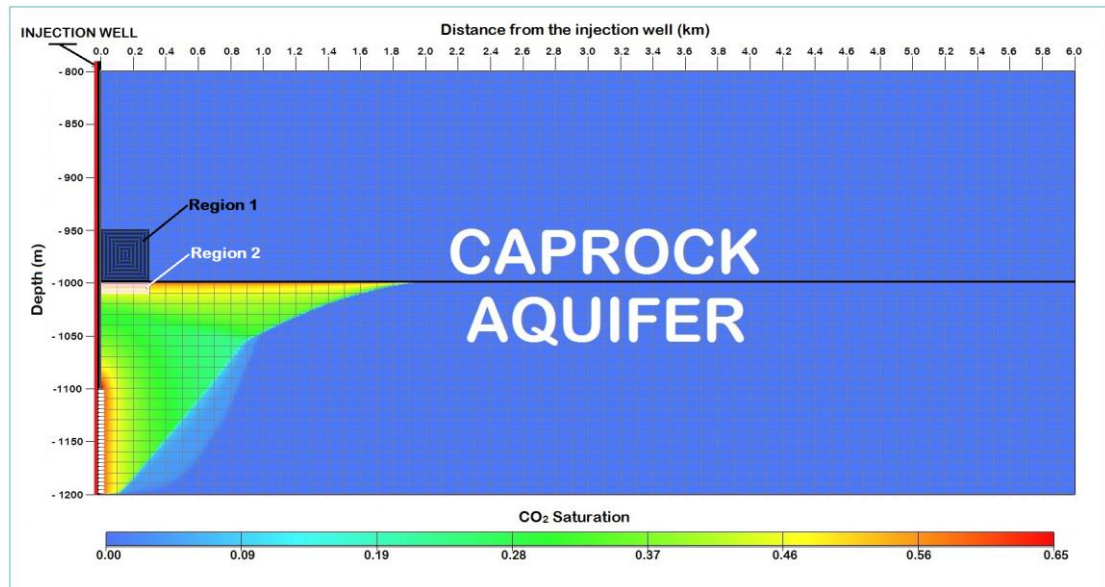


Fig. 2: CO<sub>2</sub> distribution at the end of the 20-year injection period for all sensitivity cases

The absence of geological barriers to vertical flow within the aquifer enhances an upward migration of the buoyant plume to the top of the aquifer. Here the rising plume is restricted by the impervious caprock and spreads out laterally beneath the caprock, moving away from the injection well. scCO<sub>2</sub> injection in the reservoir induces fluid pressure that increases monotonically with time. The results show a decline in the injection rate from approximately the 11<sup>th</sup> year of CO<sub>2</sub> injection due to the pore fluid pressure reaching the well control pressure. The rate of gas injection in the aquifer is the same and constant for all cases pre-decline. This is predictable since all cases possess the same aquifer properties. Post-decline of the injection rate, however, shows a negligible difference in curvature among the following set of cases: (BASE; CASE3\_50m; CASES with transition zone thickness of 0.1m & 1m), and (CASE1\_10m, 20m; CASE2\_10m, 20m, 50m; CASE3\_10m, 20m; CASE4\_10m, 20m), which is highlighted by the representative cases: BASE and CASE1\_20m, respectively in Fig 3b. This variability in injection rate results from varying permeabilities at the base of the caprock with could enhance or diminish fluid flow through the porous matrix as the injected gas migrates to the top of the reservoir. The degree to which these cases enhance the cumulative injection of CO<sub>2</sub> within simulated parameters is portrayed in Fig 3a. However, an indistinguishable pressurisation profile is observed within Region 2 for all the cases (Fig 3c), suggesting the irrelevance of caprock heterogeneities on aquifer pressurisation during CO<sub>2</sub> injection.

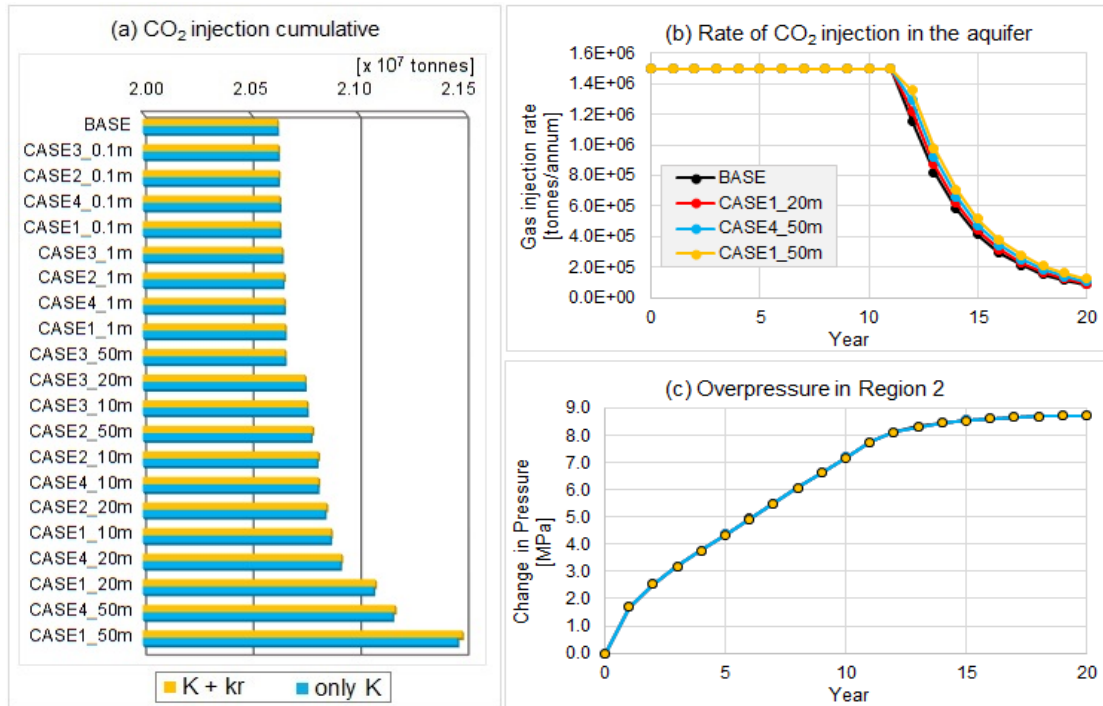


Fig 3: Plots showing a) cumulative CO<sub>2</sub> injected at the end of 20-year simulation, b) representative curves for CO<sub>2</sub> injection profile in the aquifer, and c) representative curve for pressure change in Region 2 for scenarios modelled with CLOSED boundary conditions.

### 3.1.1 Pressure evolution in the caprock

Overpressure (i.e. change in pore pressure) occurs in the caprock formation due to the coupled hydromechanical effect that occurs during CO<sub>2</sub> injection into the underlying aquifer, resulting in the vertical displacement of overpressure from the storage formation to the seal formation (Niemi et al., 2017). Unlike the pore fluid pressure profile in Region 2 (Fig. 3c), the increment of pore pressure in Region 1 over the injection period is not the same for all cases modelled. Pressure propagation in Region 1, however, is slower than in Region 2 due to the contrast in permeability between the two formations. The magnitude of overpressure reported in Region 1 for each description of sedimentary heterogeneities, i.e. “ $K + k_r$ ” and “only  $K$ ”, show higher values for cases with defined heterogeneity in intrinsic permeability ( $K$ ) and relative permeability ( $k_r$ ) functions (Fig 4). This suggests a misrepresentation of heterogeneity when it is simply described by static petrophysical properties, such as porosity and permeability, in flow models.

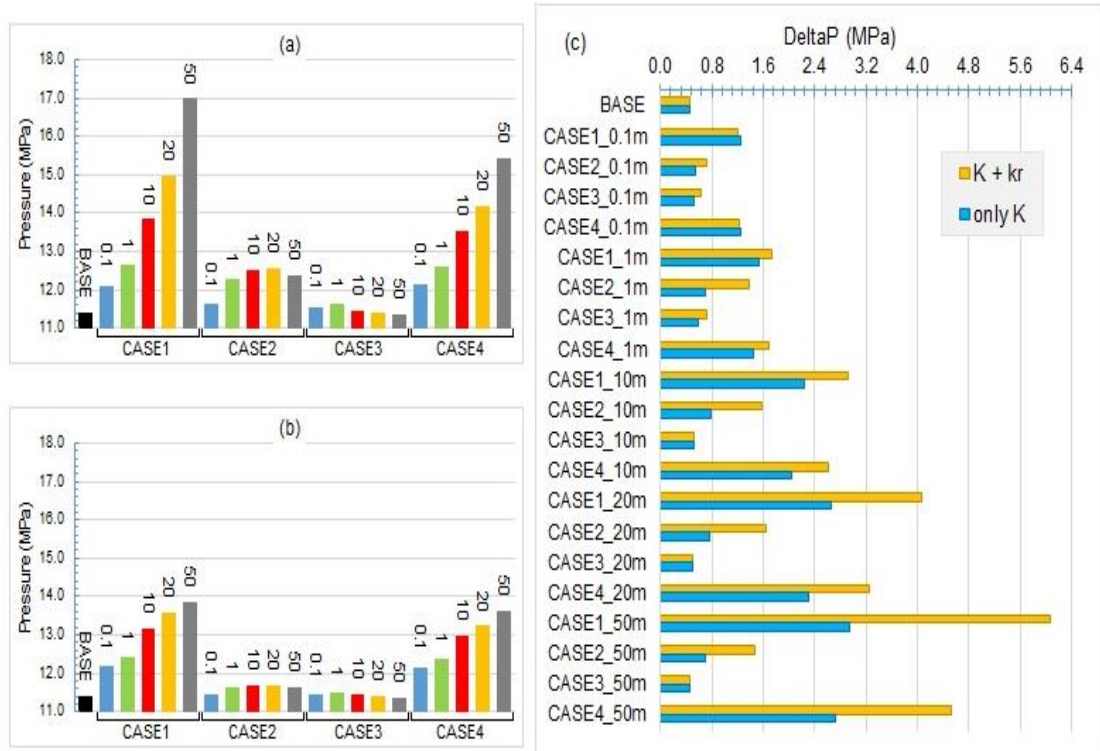


Fig. 4: Average pressure in Region 1 at the 20<sup>th</sup> year of injection for caprock heterogeneities represented by a)  $K + k_r$ , b) only  $K$ , and (c) change in pressure for both scenarios.

Numerical output of pressure data in Region 1 for both scenarios is observed to have a wider range for peak pressure values in CASES 1 & 4 from the BASE case, in comparison to CASES 2 & 3. This is largely attributed to the sequence and width of coarser or finer lithologies at the lowest part of the transitional interface. This study refers to this phenomenon as the “stacked-width” i.e. the total thickness of coarse- or fine- textured strata occurring sequentially at the base of the caprock. The stacked-width for each case is portrayed in Table 4.

CASE	Transition zone thickness (m)	Stacked-width	
		Thickness (m)	Description
1	0.1	0.06	Coarser strata
	1	0.6	
	10	6	
	20	12	
	50	30	
4	0.1	0.03	Finer strata
	1	0.3	
	10	3	
	20	6	
	50	15	
2	0.1	0.04	Finer strata
	1	0.4	
	10	4	
	20	8	
	50	20	
	0.1	0.03	

3	1	0.3	
	10	3	
	20	6	
	50	15	

Table 4: Stacked-width for coarser- or finer- strata for each case

A comparison of the average pressure in Region 1 for all cases, based on the stacked-width at the lowest part of the transitional interface, suggests that the type and width of stratum at the lowest part in caprock formation will dictate the rate of pressure diffusion into the sealing formation. In Fig. 4 we see a corresponding trend between the degree of pressure propagation into the caprock and the stacked-width in both “ $K + k_r$ ” and “*only K*” scenarios, with higher values highlighted for coarser stacked-widths. The influence of “stacked-width” is further illustrated in Fig. 5, which describes pressure propagation along the caprock, at reference depth of 990 m (i.e. 10 m above the reservoir-seal interface). This show that an increase in the stacked-width of coarser caprock lithologies, i.e. clayey sandstone, sandy siltstone and siltstone, has a direct influence on the magnitude of pressure that diffuses from the aquifer into the first few metres of the overlying caprock. In both scenarios, i.e. “ $K + k_r$ ” and “*only K*”, the pressure profile along the reference depth (i.e. -990 m) is commensurable in magnitude for caprock showing normal gradation (i.e. CASE 1 & 4) within 0.1m- and 1m-thick transition zones. Pressure curves for both cases become discernible within transition zones  $\geq 10\text{m}$ .

The pressure profile within the injection zone (i.e.  $r \leq 500$  m) for both cases differ distinctively from that for a caprock with no basal transition zone (i.e. BASE case). Magnitudes of pressure for CASE 1 & 4 are also higher than CASE 2 & 3 (i.e. caprocks showing reverse gradation) within the injection zone for all transition zones depicted. This demonstrates the capacity to which normal gradation at the base of the caprock influences the pressure character during gas injection, indicating the precedence of normal grading effects over inverse grading effects on pressure propagation. We see that reverse gradation at the base of the caprock (CASE 2 & 3) also show pressure profiles within the injection zone that differ from the BASE curve. These pressure curves, however, tend to converge towards the BASE curve more readily for “*only K*” scenarios than for “ $K + k_r$ ” scenarios. Consequently, the exclusion of relative permeability heterogeneities during such modelling exercise could easily give the notion that reverse gradation in the transition zone has negligible effects on caprock pressurisation in comparison to the absence of a basal transition zone. This further accentuates the relevance of relative permeability functions in reservoir simulations as portrayed by Onoja and Shariatipour (2018) and Mori et al. (2015).



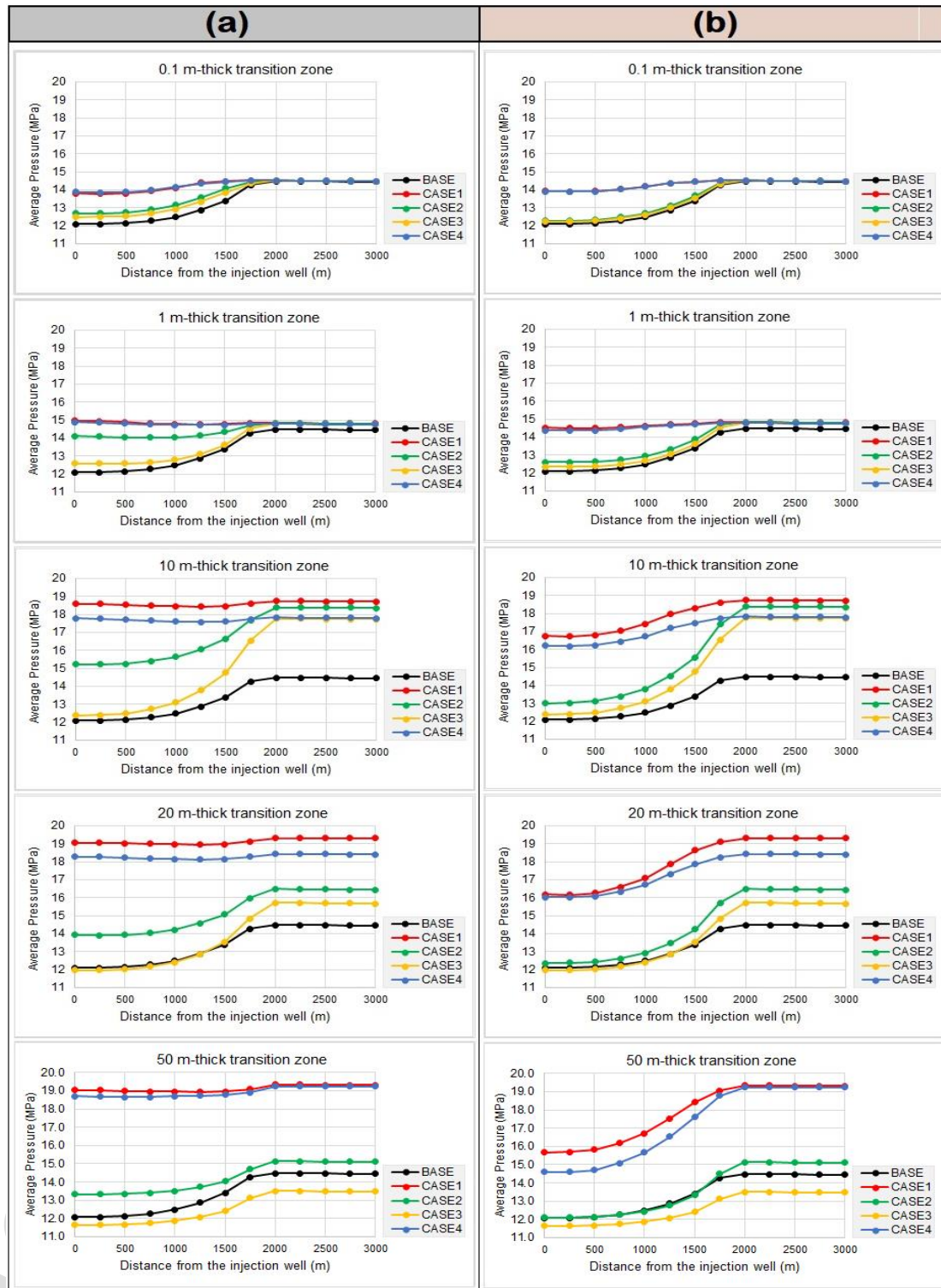


Fig. 5: Pressure profile along the caprock (depth = -990 m) of a CLOSED-system for varying transition zone thickness in caprock heterogeneities represented by a)  $K + k_r$ , b) only  $K$ .

Over the 20-year  $scCO_2$  injection period, the modelling exercise indicates that the average pressure along the reference depth (i.e. -990 m) is lower in the region overlying the injection zone (i.e.  $r \leq 500$  m) for individual cases in “ $K + k_r$ ” and “only  $K$ ” scenarios. Corresponding pressure profile for each case peaks at about 2000 m from the injection well and maintains an approximately constant value beyond this range along the reference depth in the caprock. This trend is attributed to the column height of the

CO<sub>2</sub> plume accumulating in the underlying aquifer, which serves as an inhibiting factor to pressure diffusion into the overlying caprock in the closed system (Fig. 6):

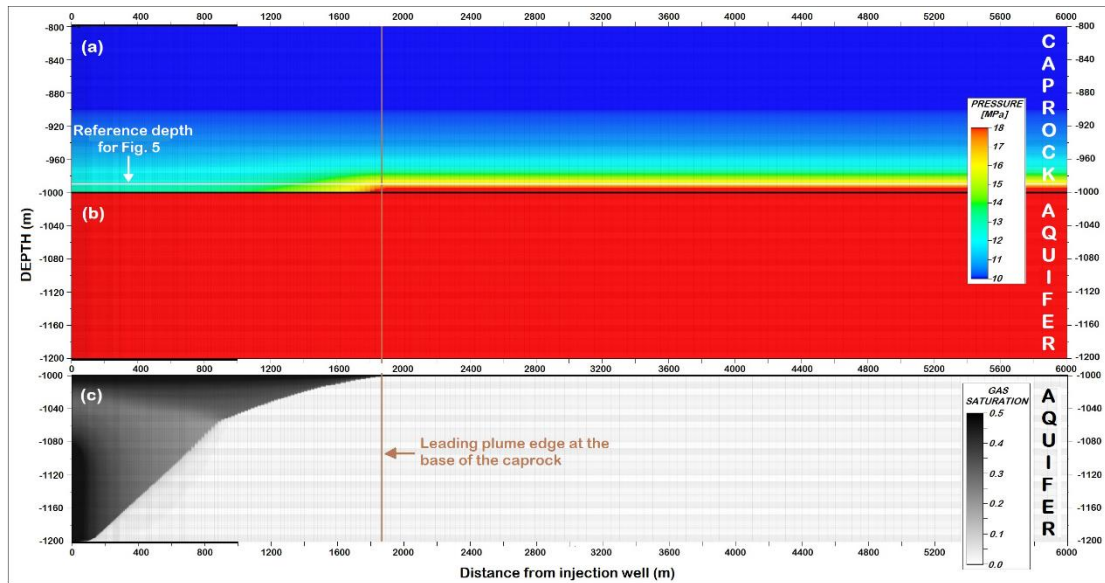


Fig. 6: 2D visualisation of the BASE case at the end of the 20-year gas injection showing (a) pressure distribution in the caprock, (b) average pressure in the aquifer, and (c) CO<sub>2</sub> saturation in the aquifer.

In analysing caprock integrity for such hydraulic systems, the caprock above the plume is a critical zone for shear failure (Vilarrasa, 2014). Fig. 5 and 6 show the leading edge of CO<sub>2</sub> plume in the aquifer coincides with the maximum values for fluid pore pressure along the reference depth in the overlying caprock formation. Qualitatively, the height of continuous CO<sub>2</sub> plume in contact with the reservoir-seal interface is portrayed to vary inversely with overpressure at the lower part of the caprock. In other words, the thickness of a buoyant CO<sub>2</sub> plume in contact with the caprock base serves to abate any pressure diffusion into the overlying caprock. This suggests that CO<sub>2</sub> injection in such a closed-system will inadvertently enhance the caprock integrity, especially at the injection zone (the near region around the injection well) in the caprock's basal stratum/strata (which is equivalent to Region 1 in this study). The observation that Region 1 is less susceptible to shear failure during injection-induced pressurisation of the caprock can be explained by Fig 7 which illustrates brine flow vectors in the modelled domain at the end of the injection period. In the closed system, lateral brine flow is restricted at the 6km boundary of the domain, resulting in the cycling of brine within the aquifer. This cycling is dominated by buoyancy effects at far-end of the model towards the 6km lateral boundary, and gravity effects on the near end of the model close to the injection well, accounting for higher pore pressures portrayed on the right half of plots in Fig 5. Nevertheless, transitional strata at the lower part of the caprock show varying effects on the magnitude of pressure that bleeds into the caprock as detailed in section 3.1.2, which only analyses results for “ $K + kr$ ” scenario due to observations in this section.



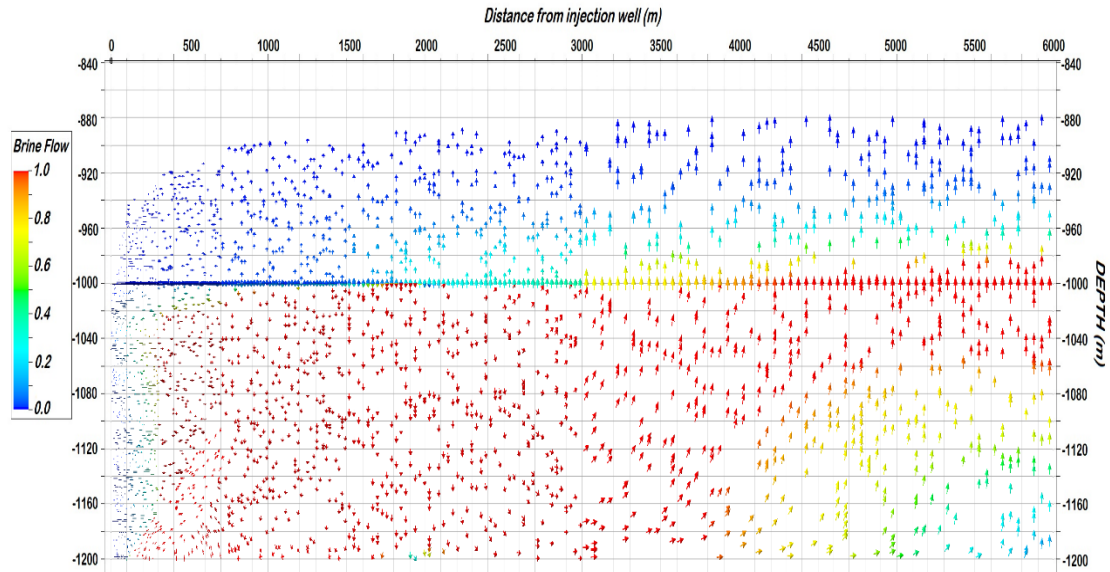


Fig 7: Volumetric brine flow vectors at the 20<sup>th</sup> year of gas injection in the CLOSED-system. NB: Color scale is the relative flow rate where 1 is the highest and 0 is the lowest. Arrows are fitted to the grid cells, resulting in reduced visibility in smaller grid cells located between 0 and 2000m.

### 3.1.2 Effects of basal transition zone on overpressure in the caprock

For 0.1m-thick transition zones, peak overpressure values in Region 1 as influenced by graded strata are no more than 0.8 MPa greater than the value for a caprock with no transition zone (i.e. BASE case). This indicates that a transition zone of 0.1 m has minimal effect on pressure change in the injection zone at the base of the caprock. As the transition zone thickens, the contrast in overpressure between the BASE and the cases showing normal gradation also increases (Fig 8). For cases that show reverse gradation, CASE 2 attains maximum overpressure values for 1 m-thick transition zones and maintains this constant pressure profile within thicker transition zones, while CASE 3 shows slight deviation from the BASE's pressure curve in transition zones  $\leq 1$  m and converges to the BASE curve for transition zones  $\geq 10$  m. The equivalent pressure profiles for BASE and CASE 3 indicate that the strata within 1 m of the caprock's base are very important for analysing the structural integrity of caprock during CO<sub>2</sub> sequestration. Recall that in CASE 3, there are ten graded beds which transition from the most compact caprock stratum (i.e. claystone) at the base, unlike CASE 2 where five graded beds transition from the sandy claystone (Table 3). The occurrence of 1m-thick claystone, the least permeable lithology in the sequence, at the base of the caprock is very crucial in mitigating the vertical displacement of fluid that should have otherwise occurred in a more permeable stratum at the caprock's base, during the fluid injection. Results portrayed in Section 3.1 indicate that the type, orientation, and thickness of strata at the lower part of the caprock plays a major role in the measure of overpressure within the critical zone of the caprock. The degree to which these strata affect pressure evolution within the entire formation hinges on their flow characteristics as represented by relative permeability functions. Fig. 8 implies that pressure evolving from the aquifer permeates the first 0.1 m of the most compact sealing lithology before the well control pressure is reached (section 3.1), and will progressively increase if and

as it vertically propagates through less compact layers. CASE 2 further suggests that the second most compact layer, sandy claystone, is more effective at a thickness  $\geq 2\text{m}$ . In contrast, CASE 1 & 4, which are direct opposites of CASE 2 & 3 respectively, show greater deviation from the BASE's overpressure profile in comparison to their inverse counterparts. This is due to the ease of pressure communication through the least compact clayey sandstone situated at the base of the transition zone, resulting in higher overpressure in CASE 1 where the least compact layer is thicker than that in CASE 4.

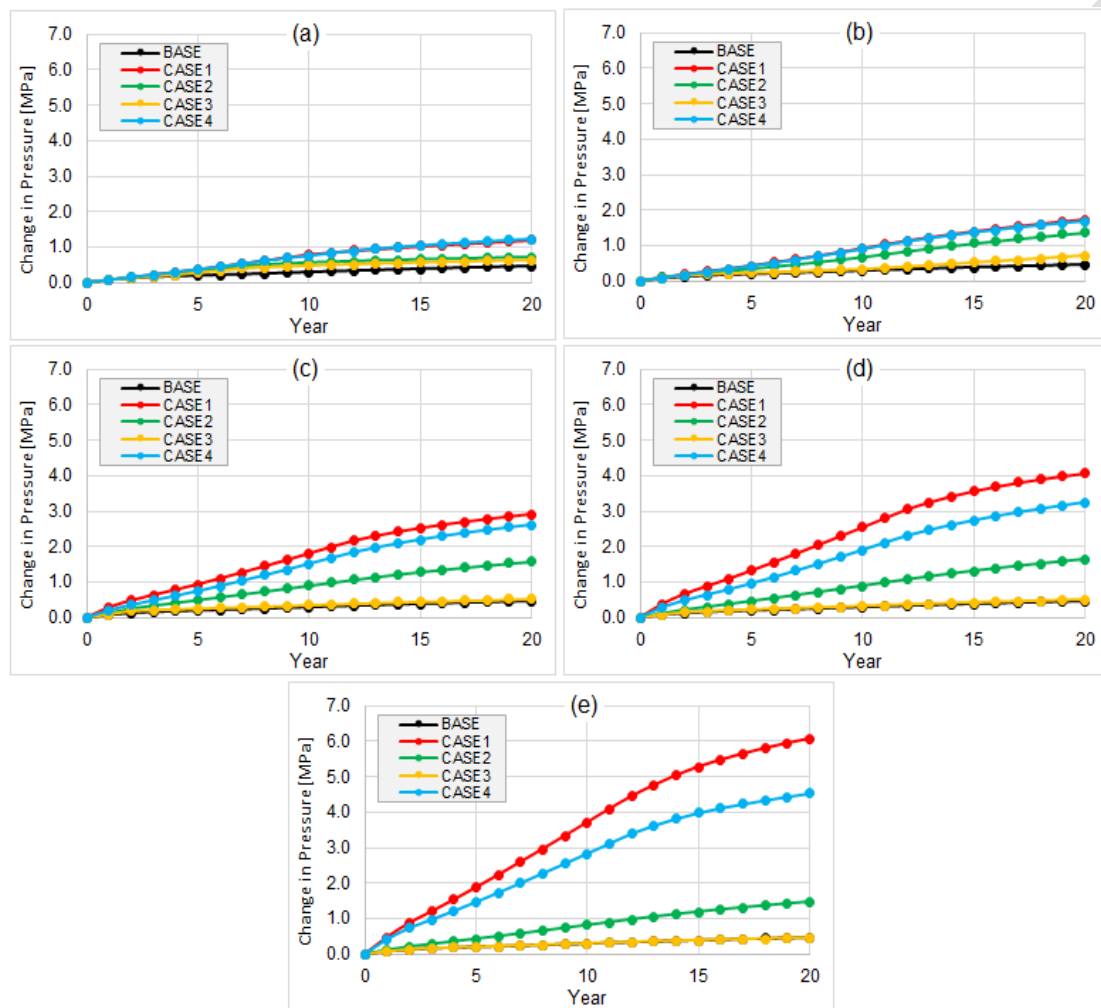


Fig. 8: Overpressure in Region 1 for cases with graded beds in a) 0.1 m-, b) 1 m-, c) 10 m-, d) 20 m-, and e) 50 m-thick transition zone.

### 3.2 Open system

Here the lateral boundary at 6km is open for fluids to escape the model domain. Simulation results show  $\text{CO}_2$  saturation, gas injection rate, and pressure profile in the aquifer to be also practically identical (Fig. 10). Unlike the closed system, there is no decline in injection rate during the 20-year gas injection in the open system due to pressure communication beyond the 6 km lateral boundary of the aquifer. This accounts for the decline in overpressure within Region 2 after an initial increase at the onset of gas injection (Fig. 10b), and corresponds to the aquifer connectivity for lateral brine migration beyond the 6 km boundary portrayed in Fig 11.

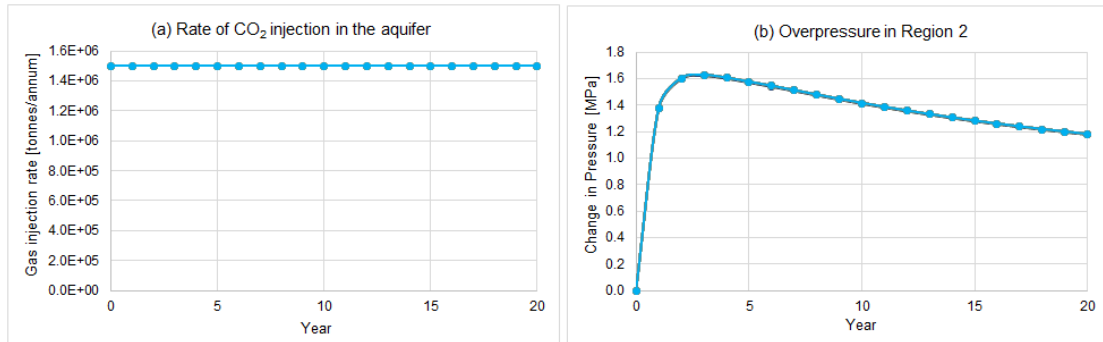


Fig. 10: Representative curve(s) for a) CO<sub>2</sub> injection rate, b) Change in pore pressure within Region 2, for cases modelled with OPEN boundary conditions

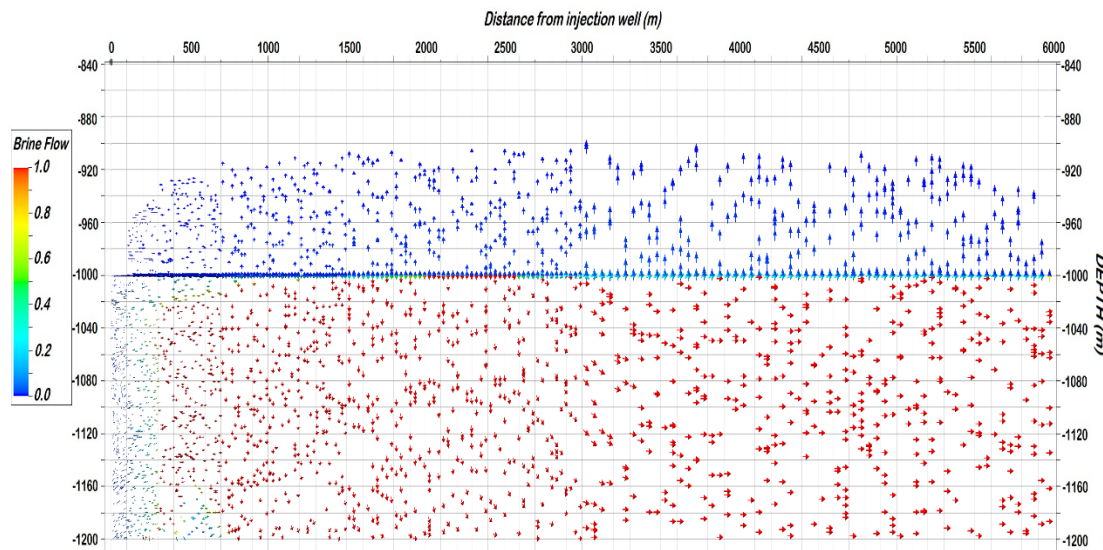


Fig. 11: Volumetric brine flow vectors at the 20<sup>th</sup> year of gas injection in the OPEN-system. NB: Color scale is the relative flow rate where 1 is the highest and 0 is the lowest. Arrows are fitted to the grid cells, resulting in reduced visibility in smaller grid cells located between 0 and 2000m.

Pressure also builds-up in the caprock of the open system as a response to CO<sub>2</sub> injection in the underlying aquifer. However, the aquifer connectivity and vast pressure communication beyond the 6 km lateral boundary results in considerably smaller magnitude of brine flow hence pressure diffusion into the caprock of the open system, in contrast to the closed system. This also explains why the pressure profiles for all cases along -990 m in “ $K + kr$ ” and “only  $K$ ” scenarios are identical (Fig. 12). Similar to closed systems, however, pressurisation at the reference depth corresponds to the degree of fluid expansion within the restricted pore space, which is higher for coarser strata than finer ones. This underpins the theory that the presence of a transition zone will have varying effects on pressure propagation regardless of the boundary conditions. Fig. 12 shows that for all cases modelled in an open aquifer, the injection zone at the base of the caprock is the most critical region for caprock integrity, which is as expected for scCO<sub>2</sub> injection scenarios. Here the pressure diffusion into the caprock can be inferred as being supported by the vertical continuity of migrating CO<sub>2</sub> plume in contact with the reservoir/seal interface (Fig. 13), contradicting the trend seen

in the closed system. This is attributed to the overall flow dynamics stipulated in Fig. 11, which enhances the vertical displacement of brine at the injection zone.

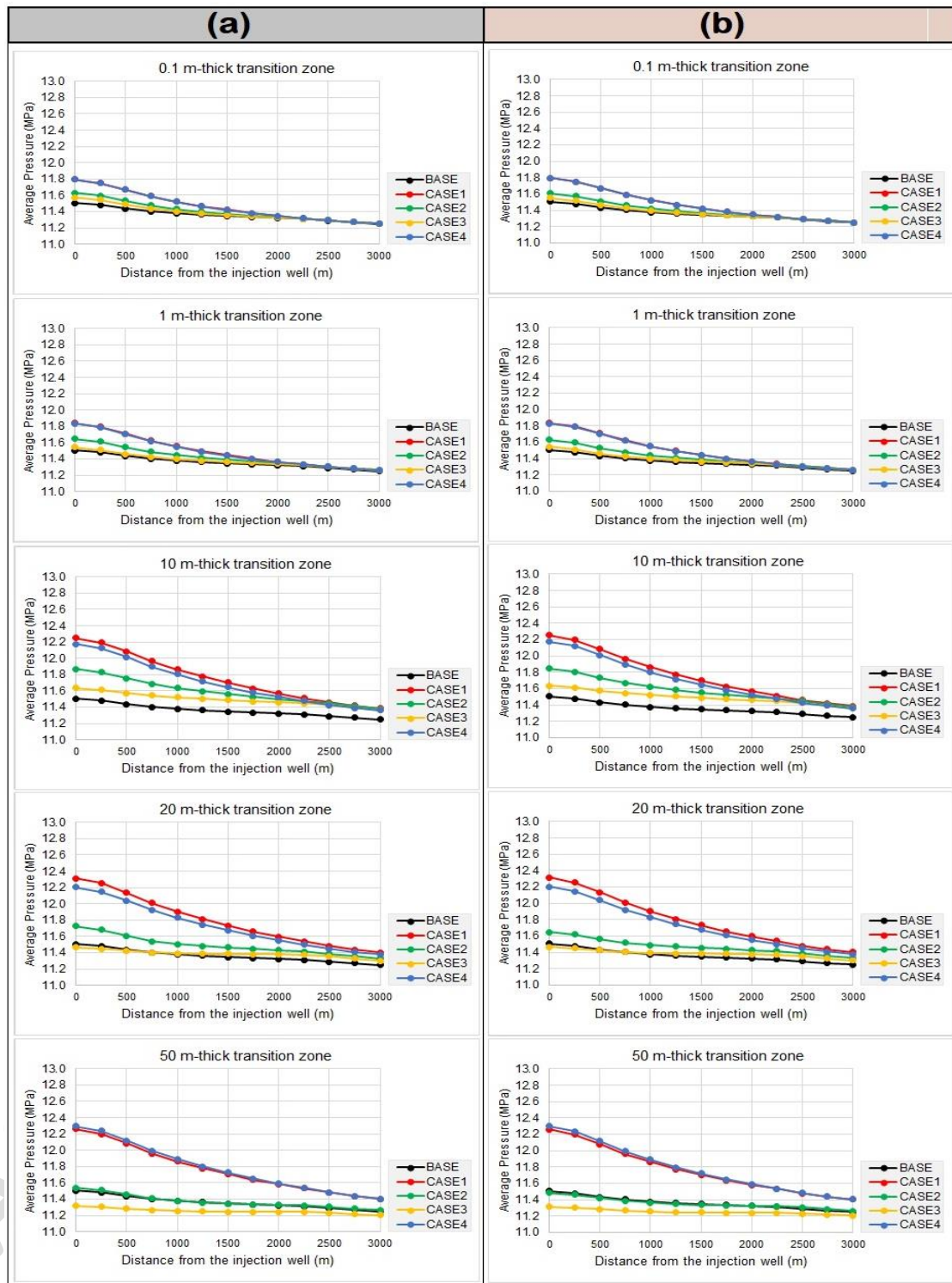


Fig. 12: Pressure profile along the caprock (depth = -990 m) of an OPEN-system for transition zone thickness of a) 0.1 m, b) 1 m, c) 10 m, d) 20 m, and e) 50 m.



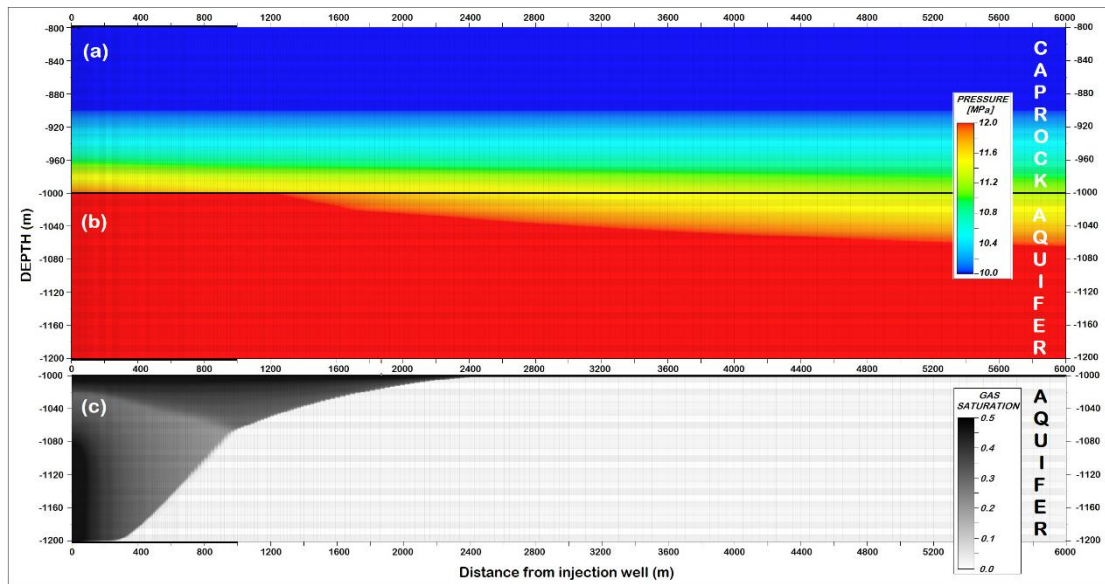


Fig. 13: 2D visualisation of the Base case at the end of the 20-year gas injection showing (a) pressure distribution in the caprock, (b) average pressure in the aquifer, and (c) CO<sub>2</sub> saturation in the aquifer.

### 3.3 Open vs Closed System

The presence of a basal transition zone in the caprock is seen to have varying effects on pressurisation in the caprock for closed and open systems. Overpressure in the caprock is however higher for closed systems due to restricted brine flow beyond the lateral edge of the model. This is because brine, which serves as a conduit for pressure migration, is pushed up into the caprock at a higher degree for closed systems than for open systems. Pressure change in the caprock will usually occur in the lower part of the seal. In Fig 14, we see the impact of a laterally continuous transition zone showing normal gradation on the height to which overpressure occurs in the injection zone at the lower part of the caprock. This reinforces the argument that such occurrence may undermine the structural integrity of the caprock during CO<sub>2</sub> sequestration. The presence of a transitional zone showing gradational changes can also increase the CO<sub>2</sub> storage capacity of the formation. At the end of the 20-year injection period, CO<sub>2</sub> migrates into the caprock and fills the interstices between pores of the rock grains. Based on dynamic material-balance computation by the simulation software, results indicate that the magnitude of pressure change in the caprock is directly related to the quantity of free CO<sub>2</sub> within the caprock (Fig 15). This is because the hydraulic system in a storage formation is limited by the compression of fluid in the modelled domain, hence the available volume for storage of CO<sub>2</sub> in the caprock is provided by the expansion of the formation in response to injection pressure. This storage capacity is dependent on the sustainable pressure build-up that a given formation seal system can tolerate without geomechanical degradation. This would suggest that for confined reservoirs that show gradation in the sealing formation, higher overpressure within the limit of the fracture pressure in the transition zone will result in further compression of the fluid, resulting in the higher storage capacity of the porous media in comparison to open reservoirs. In numerical simulations, this assertion is mostly applicable for

gradational changes that are duly accounted for by relative permeability functions in the reservoir model (Onoja and Shariatipour, 2018).

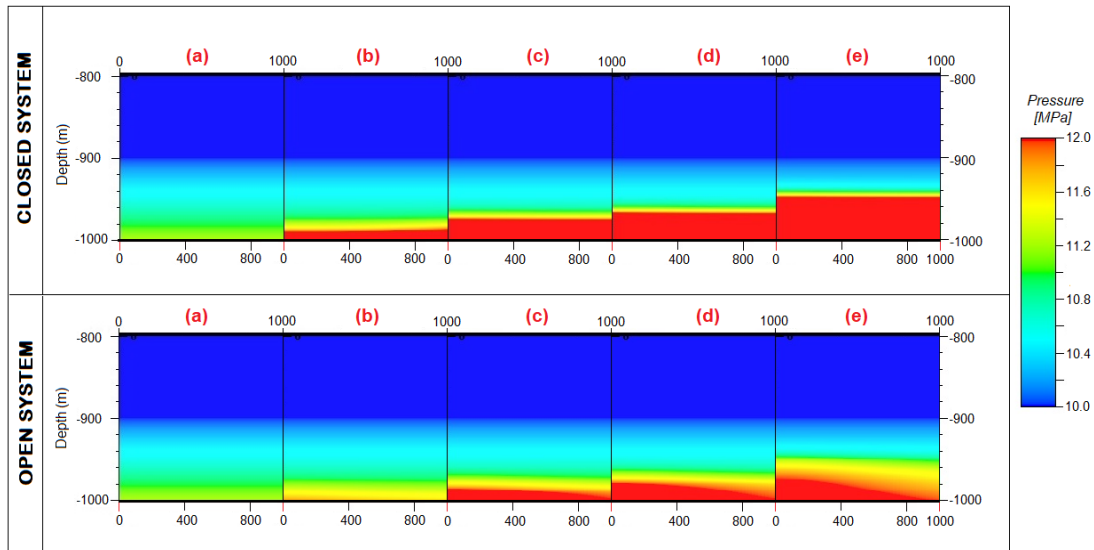


Fig. 14: Pressure distribution in the caprock between the injection well and 1000m in a) all cases before CO<sub>2</sub> injection, and b) the BASE case, c) CASE1\_10m, d) CASE1\_20m, e) CASE1\_50m at the end of CO<sub>2</sub> injection.

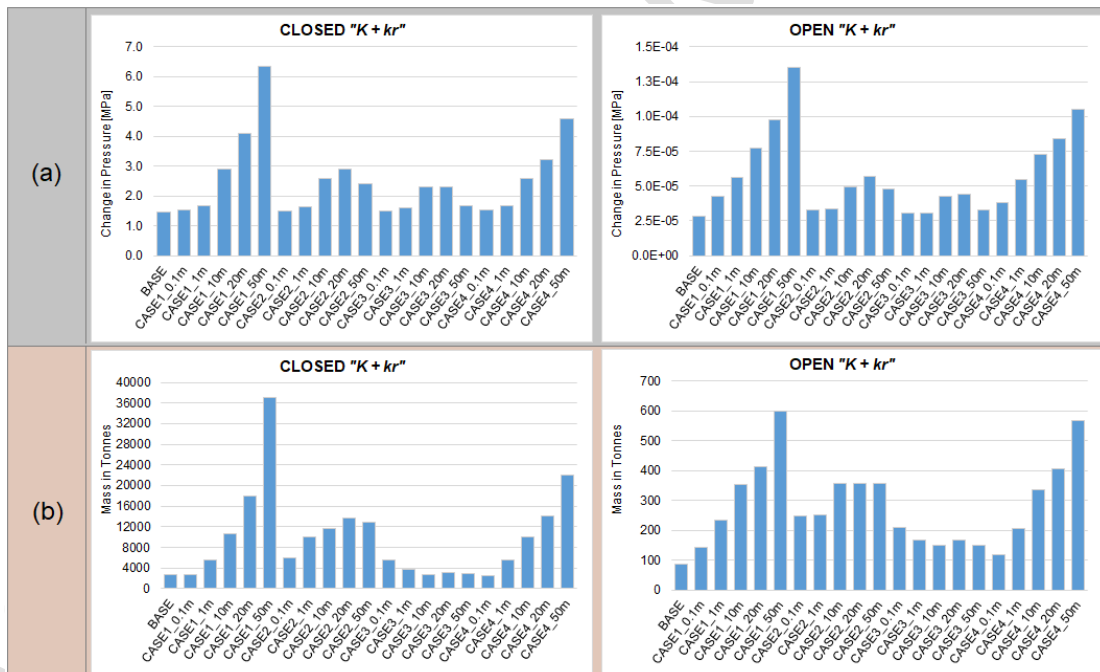


Fig. 15: Comparison of simulated outputs in the caprock of the CLOSED- and OPEN-system for a) overpressure, and b) quantity of CO<sub>2</sub> in free form.

To check the applicability of the pressure profile for closed systems confined at 6km boundary (Fig. 6) to systems with lateral boundaries beyond 6 km (Fig. 6), numerical simulations are conducted for a representative example of 1m-thick basal transition zone in modelled domains with radial boundaries of 10 km, 25 km, 50 km, and 100 km (Fig. 16). The results illustrate that closed boundaries  $\leq 10$  km tend to support the pressurisation regime described in Section 3.1.1 while those at distances  $\geq 25$  km

describe pressure profiles similar to open flow systems. This can be attributed to the considerably larger pore volume now available for brine flow within lateral boundaries  $\geq 25$  km. Regardless of boundary conditions, transitional strata at the base of a caprock show pressure profiles for the seal that differ from those without a basal transition zone.

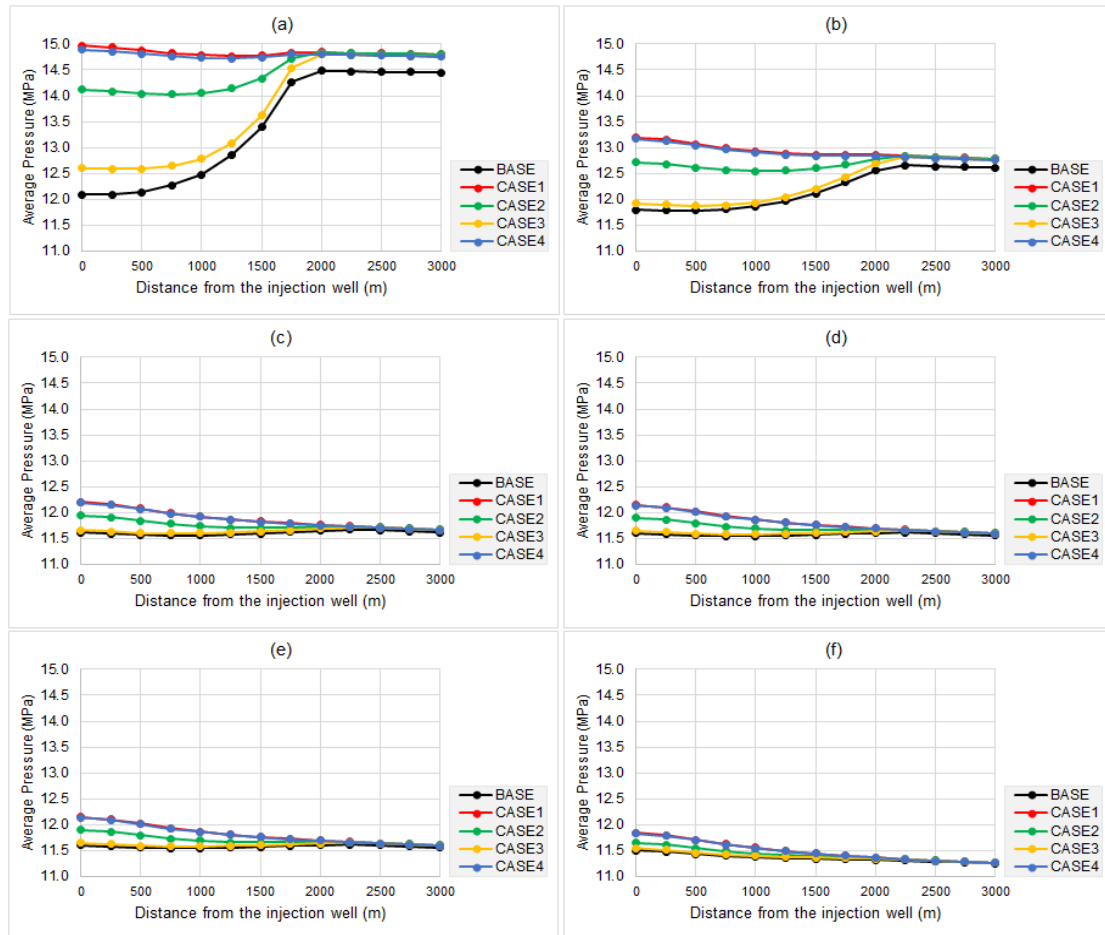


Fig. 16: Pressure profile along the caprock (depth = -990 m) for 1m-thick transition zone in radial domains modelled with no flow conditions at a) 6 km, b) at 10 km, c) 25 km, d) 50 km, e) 100 km, and flow conditions at f) 6 km from the injection well.

#### 4. Summary and conclusion

The goal of this modelling study was to explore how a basal transition zone in a sealing formation will affect CO<sub>2</sub> sequestration using relative permeability functions to describe various lithologies within the model. Empirically derived constitutive models of  $P_c$ - $S_w$ - $k_r$  based on van Genuchten-Mualem-Corey functions were used as inputs to the multiphase code ECLIPSE 100 to simulate supercritical CO<sub>2</sub> injection in a saline aquifer. Multi-phase flow characteristics for different siliciclastic lithologies were obtained using the pore size distribution index as a basic input. This study used the information on pressure distribution within the sealing formation to highlight the impact of gradational changes in the caprock's base on its structural integrity and storage capacity. The magnitude of pressure distribution was determined through numerical simulation of the multiphase flow and multicomponent transport of CO<sub>2</sub> and brine in a hypothetical saline aquifer. From the results we can infer that the presence of a basal transition zone with a thickness that transverses the region where overpressure is

expected to occur in the caprock is significant for storage capacity estimation as well as failure analysis. These results emphasise the relevance of relative permeability functions in reservoir simulations, as well as the impact of representing varying flow characteristics resulting from gradational changes, should they occur, on a subsequent geomechanical analysis.

Overpressure resulting from injection only affects the first few metres of the lower part of the whole caprock. Consequently, the presence of gradational changes at the base of the seal may allow more pressure bleed-off into the caprock. This pressure build-up in excess of the initial hydrostatic pressure will cause a higher loading at the critical zone for seals with a basal transition unit than those without. Hence, the additional stress change at the base of the seal, which will otherwise be unaccounted for in a caprock without a basal transition unit, could lead to rock failure (Orlic et al., 2011). However, based on the magnitude of pressure change observed from the simulations, it is not possible to come to a general conclusion in regard to the influence of the transition zone on caprock integrity. Nevertheless, the additional stress change observed at the critical zone will need to be taken into consideration during hydromechanical analysis. Additionally, the pressure build-up resulting from CO<sub>2</sub> injection in porous geological media changes the stress field and induces an expansion of the media. As such, the appropriate representation of flow characteristics in modelled lithologies is vital in evaluating the dynamic storage capacity of CO<sub>2</sub>. This further accentuates the need for adequate representation of small-scale geological heterogeneities in large-scale CO<sub>2</sub> sequestration modelling.

Little experimental data is currently available on scCO<sub>2</sub>-brine flow characteristics in deep saline aquifers. This is mainly due to the fact that constitutive capillary and relative permeability functions are highly site specific and experimental validation is time consuming. With this understanding, predictive reservoir models will have continued dependence on empirical models to characterise  $P_c$ - $k_r$ - $S$  relationships, hence the need for improved parametrisation. The present study investigates small-scale heterogeneities under the simplifying assumption of lateral continuity of the graded lithologies. Further work should be focused on investigating the implications of spatial distributions of such heterogeneities and other sedimentary heterogeneities on CO<sub>2</sub> storage and security. In addition, the general applicability of the parametrisation scheme used to describe  $P_c$ - $k_r$ - $S$  relationships in this work needs to be rigorously tested against available experimental data.

### **Acknowledgements**

The authors would like to thank the Centre for Fluid and Complex Systems, Coventry University, for the financial support, and Schlumberger for the use of its ECLIPSE and Petrel software. John Williams and Hayley Vosper are publishing with the permission of the Executive Director, British Geological Survey (NERC).



## References

- Alkan, H., Cinar, Y., Åcælker, E.B., 2010. Impact of Capillary Pressure, Salinity and In situ Conditions on CO<sub>2</sub> Injection into Saline Aquifers. *Transp. Porous Media* 84, 799–819. <https://doi.org/10.1007/s11242-010-9541-8>
- Amann-Hildenbrand, A., Bertier, P., Busch, A., Krooss, B.M., 2013. Experimental investigation of the sealing capacity of generic clay-rich caprocks. *Int. J. Greenh. Gas Control* 19, 620–641. <https://doi.org/http://dx.doi.org/10.1016/j.ijggc.2013.01.040>
- Amann-Hildenbrand, A., Krooss, B.M., Harrington, J., Cuss, R., Davy, C., Skoczylas, F., Jacobs, E., Maes, N., 2015. Gas Transfer Through Clay Barriers, in: Tournassat, C., Steefel, C., Bourg, I., Bergaya, F. (Eds.), *Natural and Engineered Clay Barriers*. Elsevier Ltd., Amsterdam, Netherlands, pp. 227–267. <https://doi.org/http://dx.doi.org/10.1016/B978-0-08-100027-4.00007-3>
- Anderson, S.T., 2017. Risk, Liability, and Economic Issues with Long-Term CO<sub>2</sub> Storage—A Review. *Nat. Resour. Res.* 26, 89–112. <https://doi.org/10.1007/s11053-016-9303-6>
- André, L., Peysson, Y., Azaroual, M., 2014. Well injectivity during CO<sub>2</sub> storage operations in deep saline aquifers – Part 2: Numerical simulations of drying, salt deposit mechanisms and role of capillary forces. *Int. J. Greenh. Gas Control* 22, 301–312. <https://doi.org/http://dx.doi.org/10.1016/j.ijggc.2013.10.030>
- Armitage, P.J., Worden, R.H., Faulkner, D.R., Butcher, A.R., Espie, A.A., 2016. Permeability of the Mercia Mudstone: suitability as caprock to carbon capture and storage sites. *Geofluids* 16, 26–42.
- Bachu, S., 2015. Review of CO<sub>2</sub> storage efficiency in deep saline aquifers. *Int. J. Greenh. Gas Control* 40, 188–202. <https://doi.org/10.1016/j.ijggc.2015.01.007>
- Bastin, J.C., Boycott-Brown, T., Sims, A., Woodhouse, R., 2003. The South Morecambe Gas Field, Blocks 110/2a, 110/3a, 110/7a and 110/8a, East Irish Sea. *Geol. Soc. London, Mem.* 20, 107–118.
- Bear, J., 1972. *Dynamics of Fluids in Porous Media*. American Elsevier Publishing Company, New York.
- Bennion, D.B., Bachu, S., 2008. Drainage and imbibition relative permeability relationships for supercritical CO<sub>2</sub>/brine and H<sub>2</sub>S/brine systems in intergranular sandstone, carbonate, shale, and anhydrite rocks. *SPE Reserv. Eval. Eng.* 11, 487–496.
- Bielicki, J.M., Pollak, M.F., Fitts, J.P., Peters, C.A., Wilson, E.J., 2014. Causes and financial consequences of geologic CO<sub>2</sub> storage reservoir leakage and interference with other subsurface resources. *Int. J. Greenh. Gas Control* 20, 272–284. <https://doi.org/http://dx.doi.org/10.1016/j.ijggc.2013.10.024>
- Birkholzer, J.T., Oldenburg, C.M., Zhou, Q., 2015. CO<sub>2</sub> migration and pressure evolution in deep saline aquifers. *Int. J. Greenh. Gas Control* 40, 203–220. <https://doi.org/http://dx.doi.org/10.1016/j.ijggc.2015.03.022>
- Birkholzer, J.T., Zhou, Q., Tsang, C.-F., 2009. Large-scale impact of CO<sub>2</sub> storage in deep saline aquifers: A sensitivity study on pressure response in stratified systems. *Int. J. Greenh. Gas Control*. <https://doi.org/https://doi.org/10.1016/j.ijggc.2008.08.002>
- Bloomfield, J.P., Goody, D.C., Bright, M.I., Williams, P.J., 2001. Pore-throat size distributions in Permo-Triassic sandstones from the United Kingdom and some implications for contaminant hydrogeology. *Hydrogeol. J.* 9, 219–230.
- Brooks, R.H., Corey, A.T., 1964. *Hydraulic properties of porous media*. Hydrol. Pap. BSI, 1990. British Standard Methods of Test for Soils for Civil Engineering Purposes. BS 1377: Part 1-9. British Standards Institution.

- Burnside, N.M., Naylor, M., 2014. Review and implications of relative permeability of CO<sub>2</sub>/brine systems and residual trapping of CO<sub>2</sub>. *Int. J. Greenh. Gas Control*. <https://doi.org/https://doi.org/10.1016/j.ijggc.2014.01.013>
- Cameron, D.A., Durlofsky, L.J., 2012. Optimization of well placement, CO<sub>2</sub> injection rates, and brine cycling for geological carbon sequestration. *Int. J. Greenh. Gas Control* 10, 100–112. <https://doi.org/http://dx.doi.org/10.1016/j.ijggc.2012.06.003>
- Carsel, R.F., Parrish, R.S., 1988. Developing joint probability distributions of soil water retention characteristics. *Water Resour. Res.* 24, 755–769. <https://doi.org/10.1029/WR024i005p00755>
- Class, H., Ebigbo, A., Helmig, R., Dahle, H.K., Nordbotten, J.M., Celia, M.A., Audigane, P., Darcis, M., Ennis-King, J., Fan, Y., Flemisch, B., Gasda, S.E., Jin, M., Krug, S., Labregere, D., Naderi Beni, A., Pawar, R.J., Sbai, A., Thomas, S.G., Trenty, L., Wei, L., 2009. A benchmark study on problems related to CO<sub>2</sub> storage in geologic formations. *Comput. Geosci.* 13, 409. <https://doi.org/10.1007/s10596-009-9146-x>
- Deng, H., Stauffer, P.H., Dai, Z., Jiao, Z., Surdam, R.C., 2012. Simulation of industrial-scale CO<sub>2</sub> storage: Multi-scale heterogeneity and its impacts on storage capacity, injectivity and leakage. *Int. J. Greenh. Gas Control* 10, 397–418. <https://doi.org/http://dx.doi.org/10.1016/j.ijggc.2012.07.003>
- Dewhurst, D.N., Aplin, A.C., Sarda, J.-P., Yang, Y., 1998. Compaction-driven evolution of porosity and permeability in natural mudstones: An experimental study. *J. Geophys. Res. Solid Earth* 103, 651–661. <https://doi.org/10.1029/97JB02540>
- Dewhurst, D.N., Yang, Y., Aplin, A.C., 1999. Permeability and fluid flow in natural mudstones. *Geol. Soc. London, Spec. Publ.* 158, 23–43. <https://doi.org/10.1144/GSL.SP.1999.158.01.03>
- Doughty, C., 2010. Investigation of CO<sub>2</sub> Plume Behavior for a Large-Scale Pilot Test of Geologic Carbon Storage in a Saline Formation. *Transp. Porous Media* 82, 49–76. <https://doi.org/10.1007/s11242-009-9396-z>
- Ducellier, A., Seyedi, D., Foerster, E., 2011. A coupled hydromechanical fault model for the study of the integrity and safety of geological storage of CO<sub>2</sub>. 10th Int. Conf. Greenh. Gas Control Technol. <https://doi.org/https://doi.org/10.1016/j.egypro.2011.02.490>
- Folk, R.L., 1974. *Petrology of Sedimentary Rocks*, 3rd ed. Hemphill's Bookstore, Austin.
- Handin, J., Hager, R., Freidman, M., Feather, J., 1963. Experimental Deformation of Sedimentary Rocks Under Confining Pressure: Pore Pressure Tests. *Am. Assoc. Pet. Geol. Bull.* 47, 717–755.
- Harrington, J.F., Horseman, S.T., 1999. Gas transport properties of clays and mudrocks. *Geol. Soc. London, Spec. Publ.* 158, 107.
- Hobbs, P.R.N., Hallam, J.R., Forster, A., Entwisle, D.C., Jones, L.D., Cripps, A.C., Northmore, K.J., Slef, S.J., Meakin, J.L., 2002. Engineering geology of British rocks and soils - Mudstones of the Mercia Mudstone Group, British Geological Survey Research Report, RR/01/02. British Geological Survey Research Report, RR/01/02, Keyworth, Nottingham.
- Howard, A.S., Warrington, G., Ambrose, K., Rees, J.G., 2008. A formational framework for the Mercia Mudstone Group (Triassic) of England and Wales, British Geological Survey Research Report, RR/08/04. British Geological Survey Research Report, RR/08/04, Keyworth, Nottingham.
- IEAGHG, 2017. 2nd International Workshop on Offshore Geologic CO<sub>2</sub> Storage,

- 2017-TR12, November 2017. IEAGHG, Cheltenham, UK.
- IPCC, 2005. IPCC Special Report on Carbon Dioxide Capture and Storage. Prepared by Working Group III of the Intergovernmental Panel on Climate Change. Cambridge University Press, Cambridge, United Kingdom.
- Kaldi, J., Daniel, R., Tenthorey, E., Michael, K., Schacht, U., Nicol, A., Underschultz, J., Backe, G., 2013. Containment of CO<sub>2</sub> in CCS: Role of Caprocks and Faults. GHGT-11 Proc. 11th Int. Conf. Greenh. Gas Control Technol. 18-22 Novemb. 2012, Kyoto, Japan. <https://doi.org/10.1016/j.egypro.2013.06.458>
- Khan, S., Han, H., Ansari, S.A., Khosravi, N., 2010. An Integrated Geomechanics Workflow for Caprock-Integrity Analysis of a Potential Carbon Storage, in: SPE International Conference on CO<sub>2</sub> Capture, Storage, and Utilisation. Society of Petroleum Engineers, New Orleans, Louisiana, USA. <https://doi.org/10.2118/139477-MS>
- Lenhard, R.J., Parker, J.C., S., M., 1989. On the Correspondence between Brooks-Corey and van Genuchten Models. *J. Irrig. Drain. Eng.* 115, 744–751. [https://doi.org/10.1061/\(ASCE\)0733-9437\(1989\)115:4\(744\)](https://doi.org/10.1061/(ASCE)0733-9437(1989)115:4(744))
- Liu, F., Lu, P., Zhu, C., Xiao, Y., 2011. Coupled reactive flow and transport modeling of CO<sub>2</sub> sequestration in the Mt. Simon sandstone formation, Midwest U.S.A. *Int. J. Greenh. Gas Control.* <https://doi.org/10.1016/j.ijggc.2010.08.008>
- Middleton, R.S., Keating, G.N., Stauffer, P.H., Jordan, A.B., Viswanathan, H.S., Kang, Q.J., Carey, J.W., Mulkey, M.L., Sullivan, E.J., Chu, S.P., Esposito, R., Meckel, T.A., 2012. The cross-scale science of CO<sub>2</sub> capture and storage: from pore scale to regional scale. *Energy Environ. Sci.* 5, 7328–7345. <https://doi.org/10.1039/C2EE03227A>
- Miri, R., 2015. Effects of CO<sub>2</sub>-Brine-Rock interactions on CO<sub>2</sub> injectivity - Implications for CCS. University of Oslo, Norway.
- Mori, H., Trevisan, L., Illangasekare, T.H., 2015. Evaluation of relative permeability functions as inputs to multiphase flow models simulating supercritical CO<sub>2</sub> behavior in deep geologic formations. *Int. J. Greenh. Gas Control* 41, 328–335. <https://doi.org/http://dx.doi.org/10.1016/j.ijggc.2015.05.023>
- Newell, A.J., Shariatipour, S.M., 2016. Linking outcrop analogue with flow simulation to reduce uncertainty in sub-surface carbon capture and storage: an example from the Sherwood Sandstone Group of the Wessex Basin, UK, in: Bowman, M., Jordan, C.J. (Eds.), *The Value of Outcrop Studies in Reducing Subsurface Uncertainty and Risk in Hydrocarbon Exploration and Production*. Geological Society of London, pp. 231–246.
- Nicot, J.-P., Oldenburg, C.M., Bryant, S.L., Hovorka, S.D., 2009. Pressure perturbations from geologic carbon sequestration: Area-of-review boundaries and borehole leakage driving forces. *Energy Procedia* 1, 47–54. <https://doi.org/10.1016/J.EGYPRO.2009.01.009>
- Niemi, A., Bear, J., Bensabat, J., 2017. *Geological Storage of CO<sub>2</sub> in Deep Saline Formations*. Springer, Dordrecht, Netherlands.
- Noy, D.J., Holloway, S., Chadwick, R.A., Williams, J.D.O., Hannis, S.A., Lahann, R.W., 2012. Modelling large-scale carbon dioxide injection into the Bunter Sandstone in the UK Southern North Sea. *Int. J. Greenh. Gas Control* 9, 220–233. <https://doi.org/http://dx.doi.org/10.1016/j.ijggc.2012.03.011>
- Okwen, R., Stewart, M., Cunningham, J., 2011. Effect of Well Orientation (Vertical vs. Horizontal) and Well Length on the Injection of CO<sub>2</sub> in Deep Saline Aquifers. *Transp. Porous Media* 90, 219–232. <https://doi.org/10.1007/s11242-010-9686-5>

- Oldenburg, C.M., Pruess, K., Benson, S.M., 2001. Process Modeling of CO<sub>2</sub> Injection into Natural Gas Reservoirs for Carbon Sequestration and Enhanced Gas Recovery. *Energy Fuels* 15, 293–298. <https://doi.org/10.1021/ef000247h>
- Onoja, M.U., Shariatipour, S.M., 2018. The impact of gradational contact at the reservoir-seal interface on geological CO<sub>2</sub> storage capacity and security. *Int. J. Greenh. Gas Control* 72, 1–13. <https://doi.org/10.1016/J.IJGGC.2018.03.007>
- Oostrom, M., White, M.D., Porse, S.L., Krevor, S.C.M., Mathias, S.A., 2016. Comparison of relative permeability–saturation–capillary pressure models for simulation of reservoir CO<sub>2</sub> injection. *Int. J. Greenh. Gas Control* 45, 70–85. <https://doi.org/https://doi.org/10.1016/j.ijggc.2015.12.013>
- Orlic, B., Heege, J. ter, Wassing, B., 2011. Assessing the integrity of fault- and top seals at CO<sub>2</sub> storage sites. *10th Int. Conf. Greenh. Gas Control Technol.* 4, 4798–4805. <https://doi.org/http://dx.doi.org/10.1016/j.egypro.2011.02.445>
- Orr, F.M., 2009. Onshore geologic storage of CO<sub>2</sub>. *Science* (80-. ). 325, 1656–1658. <https://doi.org/10.1126/science.1175677>
- Peters, E., Egberts, P.J.P., Loeve, D., Hofstee, C., 2015. CO<sub>2</sub> dissolution and its impact on reservoir pressure behavior. *Int. J. Greenh. Gas Control* 43, 115–123. <https://doi.org/http://dx.doi.org/10.1016/j.ijggc.2015.10.016>
- Rutqvist, J., Tsang, C.-F., 2002. A study of caprock hydromechanical changes associated with CO<sub>2</sub>-injection into a brine formation. *Environ. Geol.* 42, 296–305. <https://doi.org/10.1007/s00254-001-0499-2>
- Rutqvist, J., Vasco, D.W., Myer, L., 2010. Coupled reservoir-geomechanical analysis of CO<sub>2</sub> injection and ground deformations at In Salah, Algeria. *Ninth Int. Conf. Greenh. Gas Control Technol.* <https://doi.org/https://doi.org/10.1016/j.ijggc.2009.10.017>
- Schlumberger, 2015. ECLIPSE SimLauncher.
- Seedhouse, J.K., Racey, A., 1997. Sealing Capacity of the Mercia Mudstone Group in the East Irish Sea Basin: Implications for Petroleum Exploration. *J. Pet. Geol.* 20, 261–286. <https://doi.org/10.1111/j.1747-5457.1997.tb00636.x>
- Shariatipour, S.M., Pickup, G.E., Mackay, E.J., 2016a. Investigation of CO<sub>2</sub> storage in a saline formation with an angular unconformity at the caprock interface. *Pet. Geosci.* 22, 203–210. <https://doi.org/10.1144/petgeo2015-039>
- Shariatipour, S.M., Pickup, G.E., Mackay, E.J., 2016b. Simulations of CO<sub>2</sub> storage in aquifer models with top surface morphology and transition zones. *Int. J. Greenh. Gas Control.* <https://doi.org/https://doi.org/10.1016/j.ijggc.2016.06.016>
- Shukla, R., Ranjith, P.G., Choi, S.K., Haque, A., 2011. Study of Caprock Integrity in Geosequestration of Carbon Dioxide. *Int. J. Geomech.* 11, 294–301. [https://doi.org/10.1061/\(ASCE\)GM.1943-5622.0000015](https://doi.org/10.1061/(ASCE)GM.1943-5622.0000015)
- Smith, S.A., Beddoe, C.J., Mibeck, B.A.F., Heebink, L. V, Kurz, B.A., Peck, W.D., Jin, L., 2017. Relative Permeability of Williston Basin CO<sub>2</sub> Storage Targets. *13th Int. Conf. Greenh. Gas Control Technol. GHGT-13*, 14-18 Novemb. 2016, Lausanne, Switz. <https://doi.org/https://doi.org/10.1016/j.egypro.2017.03.1425>
- Standing, M.B., 1975. Notes on relative permeability relationships.
- Stow, D.A. V, Piper, D.J.W., 1984. Deep-water fine-grained sediments; history, methodology and terminology, in: Stow, D.A. V, Piper, D.J.W. (Eds.), *Fine-Grained Sediments: Deep-Water Processes and Facies*. Geological Society Special Publication, London, pp. 3–14.
- Trefethen, J.M., 1950. Classification of sediments. *Am. J. Sci.* 248, 55–62.
- USDA, 1987. Soil Mechanics Level I, Module 3: USDA Textural Soil Classification. United States Department of Agriculture, Soil Conservation Service.
- Van Genuchten, M.T., 1980. A closed form equation for predicting the hydraulic

- conductivity of unsaturated soils. *Soil Sci. Soc. Am. J.* 44, 892–898.
- Vilarrasa, V., 2014. Impact of CO<sub>2</sub> injection through horizontal and vertical wells on the caprock mechanical stability. *Int. J. Rock Mech. Min. Sci.*  
<https://doi.org/https://doi.org/10.1016/j.ijrmms.2014.01.001>
- Williams, J.D.O., Gent, C.M.A., Fellgett, M.W., Gamboa, D., 2018. Impact of in situ stress and fault reactivation on seal integrity in the East Irish Sea Basin, UK. *Mar. Pet. Geol.* 92, 685–696.  
<https://doi.org/10.1016/J.MARPETGEO.2017.11.030>
- Yamamoto, H., Doughty, C., 2011. Investigation of gridding effects for numerical simulations of CO<sub>2</sub> geologic sequestration. *Int. J. Greenh. Gas Control.*  
<https://doi.org/https://doi.org/10.1016/j.ijggc.2011.02.007>
- Yang, Y., Aplin, A.C., 2010. A permeability–porosity relationship for mudstones. *Mar. Pet. Geol.* 27, 1692–1697.  
<https://doi.org/http://dx.doi.org/10.1016/j.marpetgeo.2009.07.001>
- Yang, Y., Aplin, A.C., 2007. Permeability and petrophysical properties of 30 natural mudstones. *J. Geophys. Res. Solid Earth* 112, 1–14.  
<https://doi.org/10.1029/2005JB004243>
- Zhang, Y., Kogure, T., Chiyonobu, S., Lei, X., Xue, Z., 2013. Influence of Heterogeneity on Relative Permeability for CO<sub>2</sub>/Brine: CT Observations and Numerical Modeling. *GHGT-11 Proc. 11th Int. Conf. Greenh. Gas Control Technol.* 18-22 Novemb. 2012, Kyoto, Japan.  
<https://doi.org/https://doi.org/10.1016/j.egypro.2013.07.241>